19th Australasian Fluid Mechanics Conference
Melbourne, Australia
8-11 December 2014

The Existence of Multiple Solutions for Rotating Cylinder Flows

M. C. Thompson[1], A. Rao[1], J. S. Leontini[2] and K. Hourigan[1,3]

[1]Fluids Laboratory for Aeronautical and Industrial Research (FLAIR)
Department of Mechanical and Aerospace Engineering
Monash University, Victoria, 3800, Australia

[2]Department of Mechanical Engineering and Product Design Engineering
Swinburne University of Technology, John St, Hawthorn 3162, Australia

[3]Division of Biological Engineering,
Faculty of Engineering, Monash University, VIC, 3800, Australia

Abstract

A rotating circular cylinder can produce a substantial lift force, whilst at the same time reducing drag to a minimal level. Amongst other things, they have been successfully used to replace sails for marine vessels, and have potential applications for MAVs. Recently, it has been shown that the flow past a rotating circular cylinder can admit multiple steady-state flow solutions, which, in turn, explains the seemingly sudden change in the lift curve as the rotation rate is increased. The current study extends that research to show that at higher Reynolds numbers, the possible flow states extend non-trivially, with the unique solution at lower rotation rates splitting into three remarkably different solution branches, with surprisingly different flow structures.

Introduction

The richly varying wake structure of the flow past a circular cylinder represents one of the most generic and beautiful flows of fluid dynamics, often taken as the representative example of more general bluff body transition. Although less studied, adding rotation to the cylinder increases the richness and complexity of the wake transitions, as shown in a number of recent studies, e.g., [5, 15, 7, 16, 6, 1, 11, 12, 13, 14]. Amongst other things, rotation breaks the centreline reflection symmetry of the flow/wake, allowing a true subharmonic wake mode to exist, and substantially alters the boundary layer/separation behaviour, leading to the suppression of vortex shedding at high rotation rates. A number of new three-dimensional transitions that do not exist for the non-rotating cylinder, occur for a rotating cylinder as the rotation rate is varied [12, 13, 11]. Of some interest, because of the Magnus effect (Prandtl [10]), rotating cylinders have been used as high lift devices replacing sails for sailing vessels (e.g., Flettner sails) and the rotation can also substantially reduce the otherwise high level of drag. Rotating cylinders have been used for flow control devices, such as to reduce/control separation at the trailing edges of bluff bodies like trucks, or to control shedding from larger cylinders and other bluff bodies (see e.g., [3, 2]).

It was shown numerically by [5] that two-dimensional shedding from a rotating cylinder disappears when the non-dimensional rotation rate $\alpha = \omega R/U \gtrsim 2$. Here, ω is the angular velocity, R the cylinder radius and U the free-stream velocity. Effectively, the rotation of the cylinder delays separation from one side of the cylinder, resulting in a very narrow wake.

For $Re = 100$, [15] examined the flow state as a function of rotation rate finding the occurrence of a new shedding mode, known as mode II shedding, for the Reynolds number range $4.85 \lesssim Re \lesssim 5.15$. The shedding frequency in this range is much lower than that for the standard Bénard-von Kármán shedding (mode I) at lower Reynolds numbers. Beyond the upper limit of the Re range, the flow returns to a two-dimensional steady state. This return to a steady state is also associated with a kink in the lift curve with rotation rate. Stojković *et al*. [16] provided a bifurcation parameter map for ($Re \leq 200$)–($\alpha \leq 6$), examining the transitions between steady and two-dimensional periodic flow. At a similar time, [7] found two steady solutions of the governing equations for high rotation rates. At $Re = 100$, [9] showed that the nature of the steady flow changes as the rotation rate is increased, showing the transition from steady mode I to steady mode II. The solutions are connected by a small loop where three steady solutions can exist at the same rotation rate. The switch between the two steady modes accounts for the seemingly discontinuous change in the lift coefficient variation with rotation rate seen previously.

More recently, further details of the parameter map have been added by [12, 13, 14], especially determining the three-dimensional transitions for the steady or periodic base states. Experimental verification of the predicted three-dimensional modes has been provided by [11], in good agreement with the numerical stability studies.

The aim of the present paper is to examine the nature of the steady flow as a function of rotation rate. Extending the work of [9] to higher Reynolds numbers shows that three separate steady solutions can be realised at high rotation rates. Unlike the low Reynolds number case explored by [9], where, in the overlap region, the three solutions appear virtually identical, at higher Reynolds numbers this is no longer true and the rotation rate range for their existence becomes very wide.

Initially, a brief description of the numerical method is provided. Note that this work follows on from previous studies [12, 13], for which domain size and resolution studies were undertaken. Following this, the low Reynolds number results of [9] are reproduced, prior to examining the more interesting behaviour at higher Reynolds numbers.

Methodology

Problem Setup

The problem consists of a two-dimensional rotating cylinder in a uniform stream. The two governing parameters are the Reynolds number, $Re = UD/\nu$, with D the cylinder diameter and ν the kinematic viscosity, and the non-dimensional rotation rate, $\alpha = \omega R/U$, as defined above.

Numerical Method

The two-dimensional steady incompressible Navier-Stokes equations govern the flow. These are solved using a varia-

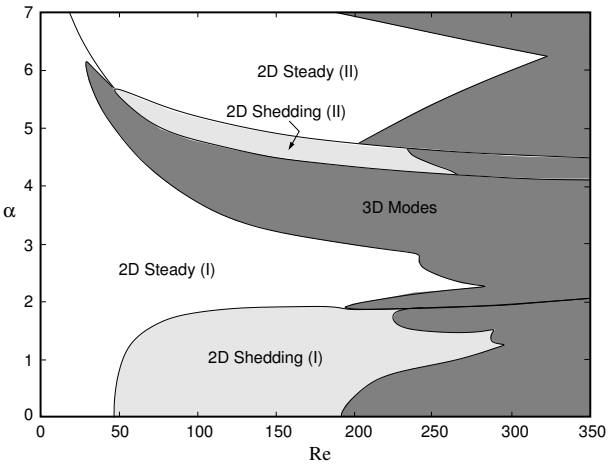

Figure 1: Simplified stability map for the wake states of a rotating cylinder. For the α–Re range shown, there are two 2D shedding regions marked by the light grey, whilst at higher Reynolds numbers the flow becomes three-dimensional (dark grey). At lower Reynolds numbers and extending to higher rotation rates, the flow remains both two-dimensional and steady.

tion of the spectral-element method [18, 19, 17, 20], which uses the penalty method to enforce the incompressibility constraint (e.g., [22]), together with Newton iteration to converge to the steady-state solution. The code has been validated and successfully employed for a number of related problems (e.g., [4, 21, 8]). The method uses a tensor-product of high-order Lagrangian interpolants to represent the velocity variation within quadrilateral macro-elements of the mesh based on the Gauss-Legendre-Lobatto quadrature points within elements. The macro-elements can have curved boundaries, allowing accurate representation of the cylinder boundary. The polynomial order can be chosen at runtime, allowing a resolution study to be performed relatively easily, as long as the macro-element mesh is constructed carefully and is sufficiently fine. Typically either 3rd or 4th order polynomials, i.e., elements with 4×4 or 5×5 points, were used for the simulations. The results are verified against those of [9], as discussed in the results section.

The computational domain was a backwards "D" shape, with the upstream and side boundaries placed $50D$ from the centre of the cylinder, situated at (0, 0), leading to a blockage of 1%. The downstream boundary is positioned at $x/D = 40$. At the upstream and side boundaries, the free stream velocity is imposed, and at the downstream boundary the velocity gradient is set to zero. An advantage of the penalty formulation is that it does not require explicit boundary conditions for the pressure. The specified rotational velocity is applied at the cylinder surface. The mesh was carefully constructed with a very high mesh point concentration at the cylinder boundary to resolve the high velocity gradients there.

At higher Reynolds number, the use of the Newton iteration approach requires a good initial starting estimate for the velocity field. This is obtained by finding the solution at a low Reynolds number and slowly incrementing the Reynolds number to reach the desired final value. For most of the runs, the solution is converged at a particular rotation rate, then that solution is used as an initial guess at the next rotation rate. Typically, it only requires a few iterations to reduce the error to machine accuracy, if the initial guess is sufficiently close.

Results

A stability map for the flow state was produced by [16] showing the two-dimensional wake state as a function of Reynolds number and rotation rate. This has been extended to show the three-dimensional transitions by [12, 13]. A simplified version of the parameter map has been reproduced in figure 1 for $0 \geq \alpha \geq 7$ and $Re \leq 350$. In general, rotation stabilises the wake against three-dimensional transition, although new modes not found in the non-rotating circular cylinder wake appear. Interestingly, the steady flow is unstable to transition from a two- to three-dimensional steady wake even at quite low Reynolds numbers ($Re < 50$) as the rotation rate is increased. At even higher rotation rates ($\alpha \gtrsim 5.5$), the steady flow state changes character and three-dimensionality is again suppressed. Note that even at $Re = 200$ there are still large rotation rate ranges where the flow remains two-dimensional. Also, of importance to the current paper, there are two different stable steady-state solutions, denoted as modes I and II. These occur at lower/higher rotation rates, respectively. The transition occurs across a narrow region in parameter space, where the stable state is type II two-dimensional periodic shedding. These states have been differentiated by whether the hyperbolic point in the wake forms in front or behind the centre of the cylinder.

Pralits *et al*. [9] examined the steady flow states at $Re = 100$, showing the existence of a very small loop in the lift–rotation rate curve, between $5.17 < \alpha < 5.21$. Over this range, three steady flow states exist, although the physical difference between these states cannot really be determined by eye. This calculation was repeated here with the results shown in figure 2. The indistinguishable results of [9] are overlaid. The loop occurs between $5.15 < \alpha < 5.19$, agreeing with [9] to better than 0.5%, with this slight difference probably due to the different blockages of the computational domains.

On increasing the Reynolds number, the range of rotation rate over which multiple solutions exists increases. The approximate limits are shown in table 1. Above approximately $Re = 185$, the righthand end of the loops appears to open, extending the turning point to beyond $\alpha = 10$. At $Re = 200$, figure 3 shows that there are three distinct steady solution branches beyond $\alpha \simeq 4.73$. While the two lower branches appear to have very similar lift force variations, they represent quite distinct solutions.

The differing flow structures are shown in figure 4 with filled vorticity contours overlaid by streamlines in the neighbourhood of the cylinder. These solutions correspond to $Re = 200$ and $\alpha = 6.5$. The first figure shows the structure for the upper branch of figure 3. The vorticity is concentrated in the vicinity of the cylinder with almost circular streamlines at small radii. The righthand figure shows the flow pattern obtained by slowly increasing the rotation rate from small values, using the previous solution as an initial guess for the next rotation rate. The vorticity is no longer localised to be close to the cylinder. In fact, at higher rotation rates, the top recirculation grows in size and extent to form a large vortical structure centred at a significant distance from the cylinder centre. The image in the centre shows the flow obtained starting from the upper branch solution using analytic continuation to traverse the lefthand turning point. Effectively, this involves using quadratic extrapolation from solutions near the turning point to project to a point around the corner. That branch can then be computed by again slowly increasing the rotation rate to higher values. The flow structure on this branch appears to be in-between the two other solutions. As before, a large amount of vorticity collects above the cylinder.

The behaviour of the drag coefficient at $Re = 200$ for higher

rotation rates is shown in figure 5. The three branches seen in the lift coefficient are also seen here. In general, the drag is very small relative to the lift coefficient for all three branches. Beyond the critical rotation rate, the lower loop drag approaches that of the upper branch at lower rotation rates, and the lower branch drag at higher rotation rates.

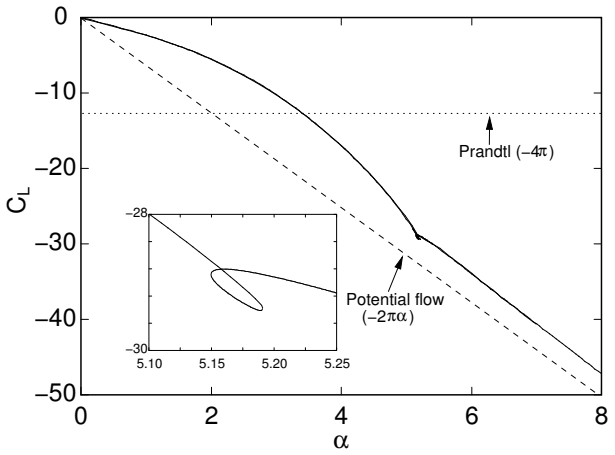

Figure 2: Variation of the lift coefficient on the cylinder as a function of rotation rate for $Re = 100$. The kink in the curve is actually a small loop, where three steady flow states co-exist. The results of [9] have been overlaid but they are indistinguishable from the current predicted variation to graphical accuracy. The inset shows a magnification of the loop structure. Also, marked are the predictions from potential flow theory and a prediction of Prandtl. Note that the predicted lift variation is insensitive to Reynolds number, except for the loop region, as can be verified from comparing the lift prediction in figure 3 below.

Range for Multiple Solutions			
Re	α_{min}	α_{max}	$\Delta\alpha$
100	5.15	5.19	0.04
120	5.03	5.11	0.08
150	4.89	5.08	0.19
175	4.80	5.14	0.34
185	4.77	5.24	0.47
200	4.73	$\gg 10$	

Table 1: Extent of rotation rate range for multiple solutions as a function of Reynolds number.

Acknowledgements

The support from Australian Research Council Discovery Grants DP0877327, DP0877517, DP130100822 and computing time from the National Computational Infrastructure (NCI), Victorian Life Sciences Computation Initiative (VLSCI), iVEC@Murdoch and Monash Campus cluster are gratefully acknowledged.

Conclusions

Although the incompressible Navier-Stokes equations do not forbid the existence of multiple solutions for the same problem parameters, for most flows this does not appear to occur. Well known counterexamples are Taylor Couette flow, for which the the number of Taylor vortices is a function of the initial conditions, and vortex-induced vibration, with the possibility of hysteretic behaviour in some circumstances. The case examined here shows that the addition of rotation to a cylinder in an open flow can increase the mathematical complexity of the solution

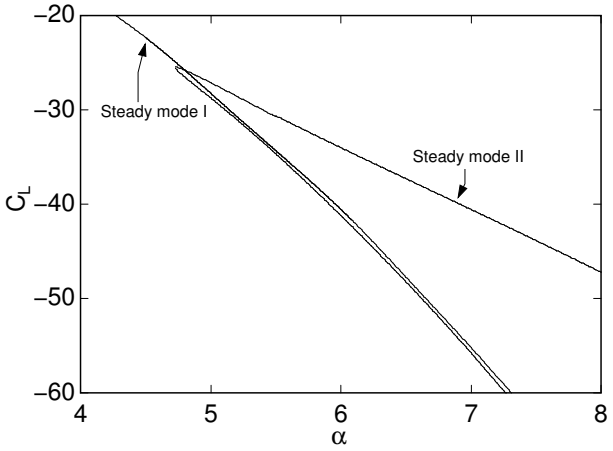

Figure 3: Variation of the lift coefficient on the cylinder as a function of rotation rate for $Re = 200$. Beyond 4.73, three steady solutions are present. The loop that exists for lower Reynolds numbers opens at the right end. Two of the solutions have almost identical lift but show distinct flow patterns.

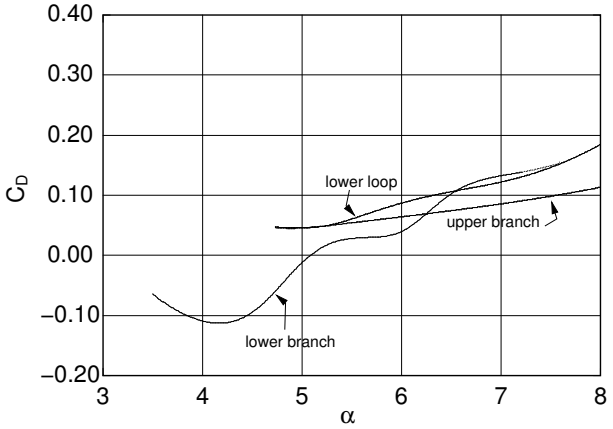

Figure 5: Variation of the drag coefficient on the cylinder as a function of rotation rate for $Re = 200$. Beyond 4.73, three steady solutions are present. Note that size of the drag coefficient relative to the lift coefficient.

topology, with high rotation allowing the existence of three distinct steady solutions. Whilst only one of these solutions is stable, it may be possible to stabilise the other using passive control strategies or another rotating cylinder to mutually stabilise the large vortex structures generated.

References

[1] Akoury, R. E., Braza, M., Perrin, R., Harran, G. and Hoarau, Y., The three-dimensional transition in the flow around a rotating cylinder, *Journal of Fluid Mechanics*, **607**, 2008, 1–11.

[2] Choi, H., Jeon, W.-P. and Kim, J., Control of flow over a bluff body, *Annual Review of Fluid Mechanics*, **40**, 2008, 113–139.

[3] Collis, S. S., Joslin, R. D., Seifert, A. and Theofilis, V., Issues in active flow control: theory, control, simulation, and experiment, *Progress in Aerospace Sciences*, **40**, 2004, 237–289.

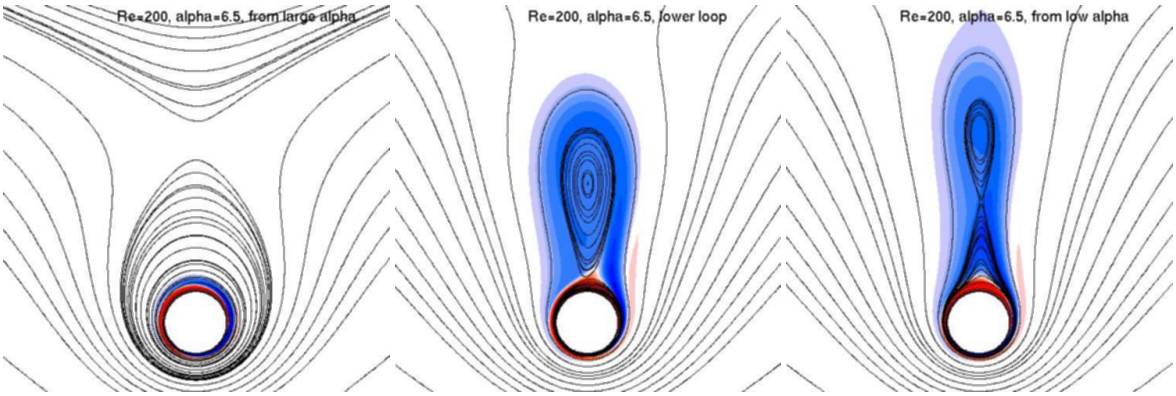

Figure 4: Three steady solutions at $Re = 200$ for $\alpha = 6.5$. Filled vorticity contours (blue(+)/red(−)) are overlaid by streamlines to show the structure. The cylinder is rotating counter-clockwise. See text for more details.

[4] Hourigan, K., Graham, L. W. and Thompson, M. C., Spiral streaklines in pre-vortex breakdown regions of axisymmetric swirling flows, *Physics of Fluids*, **7**, 1995, 3126–3128.

[5] Kang, S. M., Choi, H. C. and Lee, S., Laminar flow past a rotating circular cylinder, *Physics of Fluids*, **11**, 1999, 3312–3321.

[6] Mittal, S., Three-dimensional instabilities in flow past a rotating cylinder, *Journal of Applied Mechanics*, **71**, 2004, 89–95.

[7] Mittal, S. and Kumar, B., Flow past a rotating cylinder, *Journal of Fluid Mechanics*, **476**, 2003, 303–334.

[8] Mununga, L., Jacono, D. L., Sorensen, J. N., Leweke, T., Thompson, M. C. and Hourigan, K., Non-newtonian shear thinning flows past a flat plate, *Journal of Fluid Mechanics*, **738**, 2014, 5–33.

[9] Pralits, J. O., Brandt, L. and Giannetti, F., Instability and sensitivity of the flow around a rotating circular cylinder, *Journal of Fluid Mechanics*, **650**, 2010, 513–536.

[10] Prandtl, L., *Application of the "Magnus Effect" to the Wind Propulsion of Ships*, Technical memorandum, National Advisory Committee for Aeronautics, 1926.

[11] Radi, A., Thompson, M. C., Rao, A., Hourigan, K. and Sheridan, J., Experimental evidence of new three-dimensional modes in the wake of a rotating cylinder, *Journal of Fluid Mechanics*, **734**, 2013, 567–594.

[12] Rao, A., Leontini, J., Thompson, M. C. and Hourigan, K., Three-dimensionality in the wake of a rotating cylinder in a uniform flow, *Journal of Fluid Mechanics*, **717**, 2013, 1–29.

[13] Rao, A., Leontini, J. S., Thompson, M. C. and Hourigan, K., Three-dimensionality in the wake of a rapidly rotating cylinder in uniform flow, *Journal of Fluid Mechanics*, **730**, 2013, 379–391.

[14] Rao, A., Radi, A., Leontini, J. S., Thompson, M. C., Sheridan, J. and Hourigan, K., A review of rotating cylinder wake transitions, *Journal of Fluids and Structures*, available online.

[15] Stojković, D., Breuer, M. and Durst, F., Effect of high rotation rates on the laminar flow around a circular cylinder, *Physics of Fluids*, **14**, 2002, 3160–3178.

[16] Stojković, D., Schön, P., Breuer, M. and Durst, F., On the new vortex shedding mode past a rotating circular cylinder, *Physics of Fluids*, **15**, 2003, 1257–1260.

[17] Thompson, M., Leweke, T. and Hourigan, K., Sphere-wall collisions: vortex dynamics and stability., *Journal of Fluid Mechanics*, **575**, 2007, 121–148.

[18] Thompson, M. C., Hourigan, K., Cheung, A. and Leweke, T., Hydrodynamics of a particle impact on a wall, *Appl. Math. Model.*, **30**, 2006, 190–196.

[19] Thompson, M. C., Hourigan, K. and Sheridan, J., Three-dimensional instabilities in the wake of a circular cylinder, *Exp. Therm. Fluid Sci.*, **12**, 1996, 190–196.

[20] Thompson, M. C., Radi, A., Rao, A., Sheridan, J. and Hourigan, K., Low-Reynolds-number wakes of elliptical cylinders: from the circular cylinder to the normal flat plate, *Journal of Fluid Mechanics*, **751**, 2014, 570–600.

[21] Wu, J. and Thompson, M. C., Non-Newtonian shear thinning flows past a flat plate, *Journal of Non-Newtonian Fluid Mechanics*, **66**, 1996, 127–146.

[22] Zienkiewicz, O. C., *The Finite Element Method*, McGraw-Hill, London, 1977, third edition edition.